Ceria-based catalysts for NO_x removal in NSR processes: a fundamental study of the catalyst modifications explored by in situ techniques

J.C. Martínez-Munuera [a], J. Giménez-Mañogil [a], Lidia Castoldi [b], Luca Lietti [b], A. García-García [a*]

[a] *MCMA Group, Department of Inorganic Chemistry and Institute of Materials, University of Alicante, Carretera de Sant Vicent del Raspeig s/n, 03690, Sant Vicent del Raspeig, Alicante, Spain.*

[b] *Laboratory of Catalysis and Catalytic Processes, Dipartimento di Energia, Politecnico di Milano, Via La Masa 34, 20156 Milano, Italy*.

Abstract

In this work, a fundamental and systematic study was conducted, leading to a better understanding of the phenomena occurring on the catalyst's surface during the NOx reduction process in NSR systems. For this purpose, ceria-based catalysts, with Cu in substitution of noble metal, have been synthesized and deeply characterized by means of XRF, XPS, *in situ* (XRD, Raman spectroscopy and DRIFTS), temperature-programmed reduction under H_2 (H_2-TPR) and under NO reaction (NO isothermal reaction + NO-TPR). The whole results show the key role of copper to promote the reducibility and the creation of oxygen vacancies, allowing a high NO consumption and fast kinetics of N_2O and N_2 formation, until the oxygen vacancies consumption takes place. The study of the surface reactions taking place in the formation of adsorbed NO_x species and the oxygen vacancies consumption with NO uptake is complex; however, a hydroxyl consumption route is found to be involved. The reduction of NO provided higher levels of N_2 at higher temperatures; also, a very high efficiency of the previously created oxygen vacancies was found for this process.

Keywords: *NO reduction; Ceria-zirconia; Copper; Surface Hydroxyl consumption; Surface Nitrites/nitrates formation; Oxygen vacancies.*

**Corresponding author. Tel.: +34 965909419; e-mail: a.garcia@ua.es*
Fax: +34 96590 3454

1. Introduction

Efficient light-duty vehicles with very low CO_2 emissions are one effective measure to help approaching the problem of global warming. For this reason, the popularization of fuel-efficient diesel and lean-burn gasoline cars is very extended. In this context, limiting NOx emissions from their exhausts is a critical question [1]. From September 2019 on all new diesel cars are required to meet a higher level of NO_x emissions regulations, regulated by the so-called RDE (Real Driving Emissions) and WLTP (Worldwide Harmonized Light-Duty Test Procedure). NO_x levels are restricted to be below the RDE limits of 168 $mg \cdot km^{-1}$. In January 2020 and 2021, the RDE NO_x limits decrease to 120 $mg \cdot mile^{-1}$ [2]. To meet these increasingly stringent emissions regulations worldwide, the development of a high performance deNO_x system results of paramount importance.

Nowadays, diesel NO_x aftertreatment methods such as urea-SCR (Selective Catalytic Reduction) and lean NO_x traps (or their combinations) are supposed to require modifications or improvements in order to fulfil these demanding regulations [3]. In this sense, vehicles having SCR as NO_x removal strategy, are expected to suffer from a 50% increase in urea consumption from present Euro 6 to meet future RDE standards. Lean NOx traps (LNTs) are presently the leading deNO_x concept for the compact lean-burn passenger cars due to requirements of space for the SCR system (urea tank and so on) [4,5]. One important drawback of the NSR concept is the decrease in NO_x conversions under high gas flow conditions and the limited operating temperature window to achieve the required levels of high NO_x removal [4,5]. As a result, several efforts are made on improving this technology as well as reducing the expensive PGM (Platinum Group Metal) contents.

Taking the above into consideration, more efficient, alternative or advanced exhaust emissions after-treatment technologies for lean-burn engines will be required. The Di-Air strategy [6–8], under development by Toyota, shows certain evidences to meet the future NO_x emission requirements under real operation conditions. The Di-Air system achieves high NO_x conversion levels (above 80%) even up to 800°C and high GHSV (Gas Hourly Space Velocity). This concept aimed at making the most of the NSR function by increasing the frequency of the rich/lean cycles though supplying the reductant over short periods, upstream of the NSR catalyst. Fast HC injection pulses achieve to maximise the fact that N_2 is formed also during a certain number of seconds

after switching from the rich to the lean period (and not only during the rich step) [9]. However, the deep knowledge on the role of each catalyst ingredient is crucial for understanding how the system runs and its further improvement.

The formulation of a NSR (NO_x Storage - Reduction) catalyst is very complex; in fact, over the alumina support, with the corresponding stabilizers (La and/or Ba), different elements are present with different functions. PGMs like Pt, Pd and Rh are responsible for oxidation/reduction reaction and alkaline and alkaline-earth metals like Ba and K are necessary to store NO_x onto the catalyst surface. Ceria-based oxides are added as Oxygen Storage compounds and can operate as "active" supports and/or co-catalysts in several important environmental applications (Three-Way Catalysts - TWCs, LNTs, catalysed soot filters, and so on.) [10,11]. CeO_2 is an essential catalyst component in the Di-Air system as well, due to the above-mentioned redox properties, since it can act as an oxygen buffer [12–14]. Under rich (fuel injection) conditions, its surface and lattice oxygen can react with hydrocarbons, CO and H_2 [12,13]. The injection of HCs is a key issue to promote a relevant reduction degree of ceria. Besides, Yoshida et al. [7] reported that the amount of generated N_2 in a NSR catalyst including the ceria component was larger than without the ceria presence under lean/rich cycles. However, the specific role of CeO_2 (and also of other components) in this context is still under debate.

Wang et al. [15] investigated the role of the ceria component in the NSR process. According to these authors, NO can dissociate on oxygen anion defects, thus filling these vacancies with oxygen anions and forming N_2; and, as pointed out by Wang et al., the carbonaceous deposits in case the catalyst was reduced by C_3H_6, are oxidized by oxygen species originated from lattice oxygen [15, 16]. Even though these findings open a new perspective on the understanding of ceria as deNO_x catalyst, additional advances on this topic would be welcome due to the urgent needs of extremely effective exhaust-emission after-treatment technologies of NO_x reduction.

Considering that NSR processes are under revision and re-evaluation, due to the lean NO_x emission control, the more stringent coming regulations make these investigations extremely challenging, owing to the catalytic materials of last generations involved, which contain more and more ceria in their formulations. The roles and influences of these ceria-based materials in the processes' dynamics should be considered. Therefore, our motivation is to conduct a fundamental study selecting model ceria/zirconia-based catalysts (without noble metals) to better understand the phenomena occurring on the catalyst during NO reduction under simplified and controlled reaction

conditions. For this purpose, we have focused our attention on the physicochemical surface and bulk transformations of the catalysts during a pre-treatment at high temperature in inert atmosphere and under H_2. These studies have been performed using *in situ* techniques, like X-ray Diffraction (XRD), Raman spectroscopy and DRIFTS (Diffuse Reflectance for Infrared Fourier Transform Spectroscopy). Then, the catalytic performances towards reduction of NO over pre-reduced catalysts have been studied, by means of micro-reactor experiments and surface characterization by *in situ* DRIFTS, providing the complementary overview of the chemistry governing the process.

2. Experimental

2.1. Catalysts preparation

Two ceria-based catalysts were prepared, namely $Ce_{0.8}Zr_{0.2}O_2$ (denoted as CZ), and Cu(2%)$Ce_{0.8}Zr_{0.2}O_2$ (named as Cu2CZ) containing 2 wt% of copper. The choice of the particular formulation $Ce_{0.8}Zr_{0.2}O_2$ for the support has been done according to our previous optimisation studies [17,18 and references herein]. A detailed description of the synthesis procedure followed for their preparation can be found elsewhere [17]. Briefly, ceria-zirconia was prepared by co-precipitation of cerium and zirconium hydroxides. For this purpose, the corresponding cerium and zirconium precursor salts $(NH_4)_2Ce(NO_3)_6$ (Panreac, 99.0% purity), and $ZrO(NO_3)_2 \cdot xH_2O$ (Sigma-Aldrich, $x \approx 6$) were dissolved together in distilled water and co-precipitated by dropwise addition of an ammonia (10%) solution. After filtration, these hydroxides were calcined at 500ºC in air for 1 hour in order to obtain the CZ catalyst.

The incorporation of copper to obtain the Cu2CZ sample was conducted by incipient wetness impregnation, by dissolving the corresponding amount of $Cu(NO_3)_2 \cdot 3H_2O$ (Panreac, 99.0% purity) in the proper volume of distilled water. Then the catalyst was dried and calcined under air at 500ºC for 1 hour.

2.2. Characterization techniques

A very complete characterization analysis of the surface, textural and structural properties of fresh CZ and Cu2CZ samples is described in depth elsewhere [17,18].

Nevertheless, some *in situ* techniques such as XRD, Raman spectroscopy, DRIFTS were employed in this work in order to investigate the possible transformations of the catalysts during some specific reaction steps.

In situ XRD device comprised a PANalytical Empyrean diffractometer, coupled to a PIXcel3D detector. Additionally, in order to keep a controlled temperature and atmosphere, an Anton Para XRK 900 reaction chamber was used. Diffractograms were recorded using the CuKα radiation (λ = 0.15418 nm) in a 2θ interval between 10º and 90º, using a step size of 0.01º every 0.24 seconds. The diffractogram acquisition was performed in 9 consecutive steps, where steps 1-5 correspond to the conditioning of the samples in Ar up to 500ºC: step 1 at 25ºC, step 2 at 300ºC after 10 min, step 3 at 400ºC after 10 min, step 4 at 500ºC after 10 min and step 5 at 500ºC after 30 min); step 6 correspond to cooling down to 350ºC under inert atmosphere; and steps 7-9 correspond to the reduction step in H_2 (2000 ppm in Ar) at 350ºC: step 7 after 30 min, step 8 after 60 min, and step 9 after cooling down at 25ºC under H_2/Ar (see description of steps in Table 1).

In situ Raman spectroscopy was performed in a LabRAM (Jobin Yvon) dispersive model, coupled to a microscope, using an infrared laser (632.8 nm, He-Ne) as radiation source and a CCD as detector (cooled by Peltier effect). The whole analysis was performed in a LinkCam FTIR600 chamber, in order to control temperature and atmosphere, with a refrigeration system. In this case, the same flow and gas concentrations were employed regarding *in situ* XRD. Spectra were collected in 4 consecutive steps, being steps 1-2 the corresponding to the conditioning in Ar: heating up to 500°C, where step 1 is at 25ºC and step 2 at 500ºC; and steps 3-4 the corresponding to the reduction in H_2 (2000ppm in Ar) at 350ºC (step 3) and cooling down to 25ºC (step 4).

All the Raman spectra presented in this work were normalized to the intensity of the main F_{2g} band. Some authors point out that changes in atmosphere and/or temperature might slightly affect the Raman bands position and width [19]. For this reason, a careful analysis, along with *in situ* XRD results, will be carried out in order to provide reasonable hypothesis to explain the phenomena taking place, considering these intrinsic difficulties.

Finally, *in situ* DRIFTS experiments were performed in a Jasco device, FT-IR 4000 Series model, comprising a Harrick high-temperature reaction chamber, coupled to a MCT detector refrigerated with liquid nitrogen. Spectra have been collected between 4000–500 cm^{-1} (4 cm^{-1} resolution and 16 scans per spectrum) during the conditioning and the reduction steps already described, and also during the catalytic tests in NO (see

below). Since Cu2CZ is a dark sample, it had to be diluted with KBr (as non-absorbent component) in order to make more visible the bands features. This characterization technique allows the identification of surface species and monitoring of the surface transformations that are taking place during the different parts of the experiment for the catalysts studied. These surface analyses are of paramount importance for the elucidation of the catalytic performance and a proper correlation with the surface and bulk properties of the catalysts. It is worth to note that at the highest temperatures (i.e. 500°C), the recorded spectra might suffer a certain signal loss. Nevertheless, this does not influence substantially on the interpretation of the DRIFTS data.

2.3. Catalytic measurements

Catalytic tests were conducted in a microreactor directly coupled to a mass spectrometer (Thermostar 200, Pfeiffer), a UV analyser (LIMAS 11HW, ABB) and a micro-gas chromatograph (3000A, Agilent). The inner diameter of the tubular quartz microreactor used was 0.6 mm. For each experiment, 60 mg of powder catalyst were mixed with 60 mg of powder quartz and placed inside the microreactor; the total flow rate was kept in 100 ml/min during the whole experiments

The catalytic systems, both CZ and Cu2CZ, were pre-reduced at 350°C, under identical conditions; then, two consecutive experiments have been performed for each sample: isothermal stage and under heating ramp experiment. In the isothermal experiment, NO (1000 ppm in He) is fed to the reactor at 50°C and 250°C until the steady state was reached. Then, the temperature was increased maintaining the NO supply (NO-TPR) up to 500°C (10°C/min).

3. Results and discussion

3.1. Structural and textural characterization

XRD and Raman characterization of both CZ and Cu2CZ show the typical fluorite structure of ceria. CuO segregated phase (tenorite) was not detected for this catalyst with a 2% of copper loading. Average crystal sizes of 5.5 and 5.9 nm were determined by the Scherrer's equation for CZ and Cu2CZ, respectively. The bulk compositions of both

catalysts were measured by XRF which showed values very close to the nominal ones. The corresponding BET surface areas yielded results of 96 and 71 m^2/g, respectively. These data, along with the trend in the decrease of the specific pore volume (0.090 versus 0.065 cm^3/g) [17], reflect a certain pore blocking in $Ce_{0.8}Zr_{0.2}O_2$ upon copper incorporation on its surface. Detailed XPS analysis revealed consistent results since a very good distribution of copper inside the accessible porosity was confirmed with copper enrichment value of 1.85 (reproducible value in several batches as reported [17]). The good copper distribution onto the support's surface was evidenced indirectly because this phenomenon is supposed to promote copper/ceria-zirconia interfacial interactions that created synergisms improving redox properties [18]. More details on the catalysts' characterization are reported elsewhere [17,18].

3.2. *In situ* characterization

The first objective of this characterization was conducting a detailed *in situ* analysis to understand the modifications of the catalysts during the pre-reduction step of the catalyst (under H_2), thus approaching in a following step the reactivity of NO over these pre-reduced solids. In this sense, catalysts were heated up to 500ºC under inert atmosphere and then were reduced in H_2 (see Experimental section).

Figure 1A depicts the different X-ray diffractograms obtained for ceria-zirconia in inert atmosphere at 500°C, and in H_2 at 350ºC. In all cases, diffraction peaks attributable to cubic fluorite structure are observed, corresponding to (111), (200), (220) and (300) reflections, characteristic of ceria [20,21]. On the other hand, these diffractograms do not show either an increase in crystal size or the appearance of new peaks (associated with the segregation/formation of new phases in the solid during these treatments). Similarly, Cu2CZ also shows a fluorite cubic-type structure. As observed in Figure 1B for Cu2CZ sample, new peaks attributable to a possible new CuO (tenorite) segregated phase are not appreciated, since they would appear at 35.5º and 38.8º [22]. Therefore, the analysis of the diffractograms shows that copper is well dispersed onto the ceria-zirconia, along the conditioning and reduction steps.

Table 1 collects the lattice parameters and average crystal sizes of the model catalysts during the different steps of the experimental procedure. If the lattice parameters and average crystal sizes are compared, considering the "fresh" sample as the first diffractogram (under Ar at 25ºC), it can be observed that during the steps of the procedure, no significant changes are detected either in CZ or in Cu2CZ, despite the thermal

treatment. It can be inferred that no remarkable distortion of the ceria-zirconia lattice is taking place and that particle sintering is not evidenced.

Nevertheless, it can be observed that during the steps of the procedure, a trend of very slight increase in the lattice parameter values is seen when increasing the temperature. According to the literature [19 and references herein], the fact that this increase is reversible once the temperature is cooled back to room temperature, for CZ, suggests that it does not relate to any major chemical change taking place within the material and rather the changes are due to the reversible thermal expansion of the fluorite lattice. Conversely, Cu2CZ shows a slightly higher value after cooling down to room temperature, which might be an evidence of chemical lattice expansion related to the formation of oxygen vacancies (0.539 versus 0.535 nm). This hypothesis is supported by additional techniques, as will be discussed below.

Figure 2A plots the *in situ* Raman spectra performed with the CZ sample for the different stages of the experiment. In the range of 550-350 cm^{-1}, a sharp and intense band appears which is attributed to the vibrational F_{2g} mode, characteristic of the fluorite-type structure of ceria, which can be considered as a symmetrical Ce-O-Ce stretch [19,23]. Additionally, a minor band at about 610 cm^{-1} also appears, which is ascribed to the oxygen vacancies in the ceria-zirconia lattice [24–26]. It should be noted that the intensity of this band barely increases after *in situ* treatment, which suggests that this sample is not easily reducible at a bulk level.

With respect to Cu2CZ, Figure 2B depicts its normalized Raman spectra in different stages. These spectra keep the main peak position in the range of 550-350 cm^{-1}, which belongs to the F_{2g} Raman mode of a fluorite-type structure. In addition, a very pronounced band adjacent to the main peak appears at around 610 cm^{-1}, attributed to the oxygen vacancies. According to the different spectra shown, important changes occur in the band intensity, associated with oxygen vacancies when thermal treatments are carried out (see Supplementary Material for additional explanations). Mainly, this band arises after finishing the pre-reduction in H_2, which is an important evidence of a considerable amount of oxygen vacancies generation in this sample, compared to its initial state. Therefore, the presence of vacancies within the sample is abundant after the reduction step, as it is clearly evidenced by Raman spectroscopy.

Since the intensity and the position of the Raman bands can be dependent on the temperature and reaction atmosphere [19], Figure 3 presents a proper comparison of the samples under the same *in situ* treatment conditions: the pre-reduction step. After pre-

reduction in H_2, it can be observed that the oxygen vacancies concentration is much higher in Cu2CZ than in CZ. In fact, the ratio between the intensity of the vacancy band and that of the F_{2g} mode can be compared, yielding the values of 0.04 for CZ and 0.26 for Cu2CZ. It is worth taking this fact into consideration, because as will be explained later, they will have a very active role in the reaction with NO [27]. The results obtained by *in situ* XRD and *in situ* Raman are perfectly in line. Indeed, Raman spectroscopy is sensitive to the formation of defects in ceria-based materials, which allows monitoring the anionic vacancies' population during the *in situ* analysis [24–26].

In situ DRIFTS provides a surface characterization of the catalysts, allowing us to obtain a better understanding of the catalysts' features. It is worth noting that in the case of ceria-based materials, the study of their surface is complex, because they present a large amount of surface species; such as several types of hydroxyl groups and carbonates of various configurations and geometry. This makes the identification and assignment of the surface groups with the corresponding DRIFTS bands a difficult task.

In Figures 4A and B the spectra recorded over CZ and Cu2CZ, during the conditioning stage under inert atmosphere, are reported. The complexity of the different surface species adsorbed on the catalysts can be verified by the presence of several bands. One of the most important characteristics of ceria-based materials (such as ceria-zirconia), is the possibility that CO_2 in the gas phase can be adsorbed in the most external porosity and it can also act as Lewis acid towards O^{2-} surface ions and OH surface groups, thus forming various carbonate species [28]. In this sense, the bands appeared at approximately 1550, 1320, 1100 and 1050 cm^{-1} are attributable to surface polydentate carbonate-type species (tridentate and bidentate), with characteristic vibration modes of the C-O bond stretch [28,29]. Therefore, the existence of superficial carbonate-like species in our ceria-based catalysts is confirmed (Figure 4).

If the characteristic zone of the carbonates species is carefully analyzed, a relevant evolution can be observed upon temperature increase in the range of 200-300ºC. In these range of temperatures, the spectra change from a clear double broad band (at approximately 1550 and 1320 cm^{-1}) to different narrower and more defined peaks. This can be attributed to transformations among different types of carbonate species during the heating process. There are also two important bands at 1050 and 1100 cm^{-1} that disappear at higher temperatures (500ºC), most likely related to polydentate/tridentate carbonate species and to bridged carbonate species, respectively [29,30]. Additionally, there are bands assigned to formate species also starting at 200ºC (as will be confirmed below, after

analyzing another region of the spectra), whose vibrational modes are ascribed to the C-O bond stretch at 1550 and 1350 cm^{-1} (asymmetric ν(CO) and symmetric ν(CO), respectively); and O-C-H bending at 1371 cm^{-1} (δ(OCH)) [29,31,32]. In general, the pre-treatment at 500ºC transforms and/or removes a part of the carbonate population present in the samples, with the exception of the most thermostable ones. For this reason, a wavelength interval without enough resolution between 1550 and 1300 cm^{-1} can be found, assignable to various types of carbonates, after this pre-conditioning.

Another relevant aspect in the catalysts under study is the huge and wide asymmetric band that covers the range of 3700-2500 cm^{-1} (Figure 5), devoted to the hydrogen bonds interactions of the water molecules adsorbed on the solid [23]. Additionally, the small band at about 3688 cm^{-1} (only visible for CZ) can be assigned to the O-H stretch mode of the OH groups coordinated with a Ce cation on the catalyst's surface (type I; terminal), according to the assignments carried out by several authors [23,30,33].

Upon temperature increase, a considerable intensity loss of the wide band associated with the adsorbed water is observed (3700-2500 cm^{-1}), which indicates the desorption of water molecules from the surface. In turn, a series of bands associated with hydroxyl groups (3750-3600 cm^{-1}) starts to become visible, especially from 200-300ºC. In the CZ, the appearance along time of the double band located at about 3630 and 3660 cm^{-1} in the hydroxyl zone is attributed to O-H bond stretch vibrations of hydroxyls (type II-B and II-A, respectively) [30,34], which are characterized of being simultaneously bonded to two cerium centers of the sample. However, in the case of II-B type hydroxyls, they have an anionic vacancy adjacent to this adsorbed group, as illustrated in Figure 6 (right). Therefore, the appearance and/or growth of the band attributed to type II-B hydroxyl groups is an indirect evidence of the generation of oxide vacancies on the catalyst's surface. The weak band observed in CZ at around 3688 cm^{-1} disappears upon temperature increase, because OH groups (type I) have a higher basic character than other hydroxyl groups, and therefore, they can be more easily eliminated [35]. The double peaks related to type II-B and II-A hydroxyls in Cu2CZ give a very broad band where it is impossible to distinguish the two contributions; therefore, an enhanced absorption of infrared radiation is taking place, which consequently decreases the detection sensitivity of these bands (even diluting the samples with KBr).

In addition, in the region between 3000-2800 cm^{-1} and at 200-300ºC (Figure 5), another set of bands intimately related to the formate species previously indicated can be

detected, since the C-H bond stretch vibration appears over 2850 cm^{-1} (ν(CH)). Moreover, another band at approximately 2930 cm^{-1} based on a combination of different vibrational modes of this species can be identified [29].

Figure 7 presents the narrow DRIFTS region between 2300-1900 cm^{-1}, where at 300-500ºC, a low intensity flat band appears at approximately 2130 cm^{-1}, which according to previous studies by Daturi et al. [27], Binet et al. [36] and other authors [23] is attributed to the forbidden electronic transition $^2F_{5/2} \rightarrow {}^2F_{7/2}$ of Ce^{3+} ($4f^1$). Although this transition is strictly prohibited for Ce^{3+} ions, it might be slightly allowed due to crystalline field effects [37]. Thus, a DRIFTS region of great interest could be defined around this band, which allows to identify the presence of anionic defects associated with Ce^{3+} at a surface level in CZ [31,36]. In the case of Cu2CZ, this band is very broad and has low intensity; however, combining this feature with the information obtained by Raman spectroscopy, i.e. that this catalyst reaches a high population of oxygen vacancies, this band can be ascribed to these vacancies formed at a moderate temperature (300ºC).

During the following stage under H_2 carried out at 350ºC (pre-reduction stage), no significant changes were observed in the spectra of the catalysts (see Supplementary Material, Figures S1-S3).

3.3. Catalytic activity

3.3.1. NO reactivity under isothermal conditions

The reactivity of NO under isothermal conditions (i.e. 50°C and 250°C) has been studied over pre-reduced catalysts.

The results of the pre-reduction in H_2 at 350°C in the case of CZ and Cu2CZ are reported in Figures 8A and B, respectively. In both cases, the consumption of H_2 and release of H_2O is observed after H_2 admission to the reactor. Note that at 350°C the reduction of CZ is very low and it is difficult to describe its behaviour; for this reason a higher reduction temperature is chosen for this system, i.e. 450°C. Indeed, in these conditions (see Figure 8C) the reduction of CZ is higher and comparable to that of Cu2CZ.

Upon H_2 admission, it is consumed with production of water; then, its concentration increases reaching the inlet value. The interaction of H_2 with ceria-based materials gives the formation of H_2O according to reaction (1):

$$2\ CeO_2 + H_2 \rightarrow Ce_2O_3 + H_2O \qquad (1)$$

It should be remarked that, for each water molecule formed, an oxide vacancy is created, while two Ce^{4+} centres must be reduced to Ce^{3+}.

Therefore, a higher water emission during the pre-reduction step necessarily implies a larger population of vacancies created in the catalyst. The copper-containing sample exhibits an enhanced reducibility at 350ºC, since it consumes a higher quantity of hydrogen (859 μmol/g_{cat}) along with a larger water generation (523 μmol/g_{cat}) than CZ at any of both reduction temperatures: CZ reduced at 350ºC presents a H_2 consumption of 212 μmol/g_{cat} and a H_2O release of 143 μmol/g_{cat}; while CZ reduced at 450ºC has consumed 344 μmol/g_{cat} of H_2 and has released 286 μmol/g_{cat} of H_2O. These quantifications are very useful to compare the reducibility of the catalysts and will be furtherly employed to estimate the amount of oxygen vacancies generated during this step, in order to be correlated with the re-oxidation of the solids and with the reduced N-products emissions when NO molecules interact with them.

The reactivity of NO over pre-reduced catalysts has been investigated at first at 50°C and results are reported in Figures 9A and B for CZ and Cu2CZ, respectively. In the case of CZ (Figure 9A), upon NO admission a small consumption of this species is observed together with the formation of small amounts of N_2O and negligible amounts of N_2. After a short time, the NO concentration reaches the steady state value, corresponding to the inlet one. Over Cu2CZ (Figure 9B), as soon as NO is admitted in the reactor (represented by the dotted line) a high NO consumption is observed along with a fast production of N_2O and N_2. When the temperature is increased at 250°C (Figures 9C and D), the qualitative behavior is reproduced for both CZ and Cu2CZ, even the amounts of N_2O and N_2 produced after interaction with NO are higher.

The quantitative analysis is compiled in Table 2, where the amounts of NO consumption along with N_2 and N_2O production are reported. It is worth highlighting that by increasing the temperature, the amount of N_2O decreases, becoming N_2 the main product. By comparing the amounts of consumed NO with the N-reduction products, it is possible to conclude that small amounts of ad-NO_x species are formed on the surface, particularly at 250ºC.

To obtain a much more complete vision of the surface transformations occurring on the catalyst during NO interaction, and thus providing consistent evidences of possible reaction routes that are taking place, *in situ* DRIFTS analysis has been performed over pre-reduced CZ and Cu2CZ catalysts. Note that being the results obtained for interaction of NO at 50°C and 250°C very similar, only the former are here reported (see corresponding Figures S4-S6 in Supplementary Materials that show the CZ spectra for NO reaction at 250ºC, as an example).

In order to properly analyze the DRIFTS spectra of the samples during the NO reaction stage, three regions of the spectra were considered: i) the region of the vacancies band, between 2300-1900 cm^{-1}; ii) the region of the hydroxyls band, between 3900-2400 cm^{-1}; and iii) the region of the carbonates species band, between 2000-800 cm^{-1}.

Figure 10 shows the DRIFTS spectra in the region of 2300-1900 cm^{-1}, where the main feature observed in these catalysts is related to the band corresponding to the oxygen vacancies. In the specific case of CZ, it is perfectly noted how the band disappears in less than 20 seconds after permutation to the NO atmosphere (Figure 10A). Meanwhile, in Cu2CZ (Figure 10B), this same transformation is more difficult to be observed (due to its intrinsic detection problems).

At higher wavenumbers, other changes related to the hydroxyl groups occur simultaneously (Figure 11). In CZ, the two bands ascribed to two types of surface hydroxyl groups disappear to form a broad rounded band from 3700 cm^{-1} to 3300 cm^{-1}. It can be correlated with the consumption of type II-A and II-B hydroxyl groups and the concomitant generation of water. On the other hand, for Cu2CZ, these transformations are hardly noticeable, probably due to the limitations already mentioned; but also, because this reaction stage probably takes place in a minor extent. It should be kept in mind that, although the conditions in the catalytic reactor and *in situ* DRIFTS reaction chamber are not comparable, the nitrogen balance, quantified in the catalytic reactor experiments, is closed.

With regard to the carbonates' region in the DRIFTS spectra (Figure 12), other transformations are also observed, specifically the appearance of a new and important band located between 1207-1176 cm^{-1}, whose intensity increases during the NO reaction, which can be assigned to N-species. It can be specifically attributed to an asymmetric vibration mode of the N-O bond by chelate or bidentate nitrites [23,33,38], as schemed in Figure 13. The evolution of a new band assigned to bridged nitrate species can be also detected for Cu2CZ. This band is detectable above 1590 cm^{-1} after several minutes in the

isothermal NO reaction stage. However, this band is partially visualized as a consequence of its overlap with bands originated by carbonate species. In any case, bands associated with nitrate species for both samples could be observed. The formation of nitrates can be explained considering the ceria lattice oxygens, which are able to oxidize the already present nitrites to nitrates, without the presence of O_2 in the reaction atmosphere [23]. This route can be represented in a very simplified way as follows (2) [38]:

$$NO_2^-{}_{(sup)} + O_{(sup)} \rightarrow NO_3^-{}_{(sup)} \qquad (2)$$

Additionally, other minimum changes are visualized. In the case of CZ sample (Figure 12A), there is a slight intensity decrease of the band at 1432 cm^{-1} during the reaction with NO, which is possibly ascribed to the shift of some surface carbonate species. And in the case of Cu2CZ (Figure 12B), at long reaction times (30 minutes) the appearance of a new band at 1876 cm^{-1} is observed, which is assigned to adsorbed nitrosyl species on copper [39].

The features already described and derived from *in situ* DRIFTS spectra during the isothermal NO reaction stage suggest that adsorbed nitrite species could be formed by interaction between NO and hydroxyl species (Reaction 3), in particular type II-A hydroxyl groups. These NO molecules are transformed into nitrites (NO_2^-) and, in turn, water is generated as a reaction product [40]. This phenomenon could be justified in a simplified way as:

$$NO + 2Ce^{4+}{-}OH^- \rightarrow Ce^{4+}{-}NO_2^- + Ce^{3+}{-}\square + H_2O \qquad (3)$$

As explained, an important generation of N_2 and N_2O is observed in the first moments of the reaction with NO for the copper-containing sample, due to the high population of anionic vacancies that are characteristic of this type of materials. These oxygen vacancies are already present at the beginning of the reaction because they were previously generated in the pre-reduction step. However, during the reaction course, the number of anionic vacancies decreases, and therefore, the amount of N-species emitted decreases progressively (becoming zero at longer times).

Regarding the reaction routes involved, the N-reduced species formation (N_2 and N_2O) could be justified by the reaction of NO with the anionic vacancies of the catalyst. Researchers such as Hadjiivanov [33] have proposed the process of converting NO to N_2O and N_2 as the following sequence of reaction stages (4-7): i) electronic transfer from the ceria surface to the NO molecule, where it interacts with the oxygen vacancy (represented in Reaction 4 as □), thus creating the anionic species postulated in (4); ii) this transient and highly reactive species can dimerize with another NO molecule in the

gas phase, generating very reactive hyponitrite species (5); iii) decomposition of the hyponitrite species could generate the oxidation of the vacancy and N_2O emission (6); and iv) N_2O could react with other oxygen vacancy to form N_2 and reoxidize the ceria (7).

$$-Ce^{3+}-\square-Ce^{3+}- + NO \rightarrow -Ce^{4+}-[NO]^{2-}-Ce^{4+}- \quad (4)$$

$$-Ce^{4+}-[NO]^{2-}-Ce^{4+}- + NO \rightarrow -Ce^{4+}-[N_2O_2]^{2-}-Ce^{4+}- \quad (5)$$

$$-Ce^{4+}-[N_2O_2]^{2-}-Ce^{4+}- \rightarrow -Ce^{4+}-O^{2-}-Ce^{4+}- + N_2O \quad (6)$$

$$-Ce^{3+}-\square-Ce^{3+}- + N_2O \rightarrow -Ce^{4+}-O^{2-}-Ce^{4+}- + N_2 \quad (7)$$

After these observations, it can be inferred that higher number of anionic vacancies in the catalyst yields to higher amounts of reduction products. In this sense, Cu2CZ presents more anionic vacancies than CZ (as confirmed by the H_2 consumption in the pre-reduction step and by the band of vacancies of the *in-situ* Raman spectra). This is in accordance with the Cu2CZ profiles (Figures 9B and D), where the release of N-reduced species takes place (closing the N-balance).

After NO interaction under isothermal condition, the NO-TPR has been performed with the purpose to study the dynamics of the reaction in a wide temperature range. In the case of CZ (Figures 9A and C), increasing the temperature the concentration of NO increases and becomes higher than the NO inlet concentration (in dotted lines). It shows that most of the NO molecules consumed at the beginning of the NO isothermal stage were adsorbed onto the ceria-zirconia surface, and were subsequently released upon heating, without being reduced. There is more NO consumption than the expected N-products released during the isothermal step. These estimations indicate, therefore, the generation of superficial nitrogen species on CZ that can be released/decomposed upon temperature increase to 500ºC. Considering both steps of the experiment, the N-balance is almost closed.

Cu2CZ presents a complex NO consumption profile after isothermal NO at 50ºC (Figure 9B), along with the emission of new N_2O (concomitant with maximum NO consumption) and N_2. It might be linked to the creation of new active sites, since simultaneous emission of water is monitored. Conversely, active sites seem to be exhausted at the end of the isothermal reaction at 250ºC (Figure 9D) and negligible N-reduction products are detected during NO-TPR. It is worth noting that the nitrogen balance is practically closed (during the isothermal phase), thus indicating the high catalytic efficiency of the process for Cu2CZ at both temperatures. In other words, practically all the NO consumed in the reaction is converted into N-reduced products (N_2

and N_2O) at 50ºC or at 250ºC. Another important aspect is that neither NH_3 nor NO_2 were detected at any moment, which contrasts with the emission of certain amounts of ammonia in the NO elimination with noble metals (Pt, Pd or Rh) by NSR process [41].

In situ DRIFTS was also performed during NO-TPR to analyze the surface modifications of the catalysts during this last stage, as shown in Figures 14 and 15. One of the main changes observed in CZ spectra is the water emission, which is due to desorption of the water formed during the isothermal NO reaction. As detected, upon temperature increase (300ºC) the wide initial band between 3700-2600 cm^{-1} disappears in favor of new bands assigned to hydroxyls. It can be assumed that the appearance of a doublet corresponding to type-II hydroxyl groups is not an evidence of hydroxyl formation during the NO-TPR stage; it could rather be devoted to an unmasking process of the signals that were hidden by the wide band of adsorbed water. For Cu2CZ (Figures 14 and 15), the decrease in the adsorbed water band and the appearance of bands assigned to hydroxyl groups are also observed, although with much less intensity. However, the maintenance of the band assigned to the adsorbed water up to 200ºC is detectable, which may suggest that water continues to be generated from the hydroxyls route.

The temperature increase is a factor that promotes the decomposition of chemisorbed N-species on catalysts' surfaces. A gradual decrease of the nitrite band (1175 cm^{-1}) was observed until disappearance above 400ºC for CZ and Cu2CZ. In addition, for Cu2CZ catalyst, other bands related to N-species could be monitored: i) the disappearance of the band at 1875 cm^{-1} related to nitrosyls adsorbed on copper sites at about 200ºC; and ii) the presence of a new band between 100-300ºC at 1259 cm^{-1}, which is probably explained as a vibrational mode assigned to the adsorption of chelated nitro species on copper cations [41-43]. Another aspect to be considered, in the case of CZ, is the evolution of very narrow bands that can be assigned to formate species (2932, 2846, 1543 and 1358 cm^{-1}), at about 300ºC; however, heating up to 500ºC causes their subsequent disappearance.

The disappearance of all the bands associated with surface N-products upon temperature increase suggests a possible decomposition/reduction of these species, giving rise to NO as emission product. This transformation could be ascribed to a possible reaction route based on the reduction of nitrates/nitrites through the presence of anionic vacancies, which would generate new NO molecules that could be reduced. According to the catalytic tests, the only N-product emitted during the NO-TPR in CZ (without copper) was NO, which is somehow in accordance.

The experimental sequence of isothermal NO reaction + NO-TPR provides a suitable combination to investigate the catalytic reactions' dynamics and the pathways governing the chemical processes. On the one hand, if some retained N-species had been created, they would have been released by decomposing/interacting upon temperature increase in a reactive atmosphere. On the other hand, the most reactive catalyst that was seen to consume or diminish their active sites at the end of the isothermal stage might create new active sites (of identical or varied nature). The main purpose of this analysis is to study the catalysts' performances and their suitability for an efficient NO elimination, where the temperature range of catalytic regeneration should be maintained.

Consumption of NO is not observed in CZ, however the emission of a certain amount of NO above the inlet level was detected, as explained above. This NO excess emission is congruent with the amount of NO adsorbed during the previous isothermal NO reaction stage. Therefore, the emission of water during the NO-TPR, which starts at about 175ºC, is consistent with the fact that during the isothermal reaction stage under NO, Reaction (3) has occurred. Accordingly, during the NO-TPR, the emission of previously adsorbed water at 50ºC is taking place. In contrast, the NO-TPR profile of Cu2CZ reveals a very important catalytic activity towards NO reduction. In this case, there is a first NO consumption, with a maximum at around 150ºC, which is coincident with the maximum emission of N_2O. It verifies a significant reduction process from NO to N_2O in the first part of the NO-TPR step. The emission of N_2 starts approximately at the maximum evolution temperature of N_2O, whose emission begins to decrease. The global quantification during the NO-TPR process determines that the N_2 emission (desired reduction product for this application) is higher than that of N_2O (Table 3). In addition, it should be remarked that water emission occurs just at the beginning of the NO-TPR stage, which tentatively could be related to water generated through the hydroxyl route (3). During the first moments of the NO-TPR stage, and starting from 175ºC, H_2O emission is increased as an additional consequence of the desorption of some previously generated water during the isothermal NO reaction stage. The fact that the so-called hydroxyl route occurs during the NO-TPR, would imply the *in-situ* generation of fresh and reactive oxygen vacancies, which interact with NO and give rise to N-reduction products. It is also worth noting that CO_2 emission is detected starting from 300ºC, along with a very similar level of N_2 emission in the final stage of the NO-TPR, together with an increase in NO consumption. These results highlight that the active sites generated during this stage can have different nature. They vary from the direct NO interaction with

the oxide vacancies to the interaction with some surface carbonates, whose shift and/or decomposition in these conditions can generate new active sites, and thus, inducing the NO interaction and the direct N_2 generation.

During the discussion reported so far, the explanation of the catalytic results was given on the basis of NO consumption, catalysts' surface modifications by chemical interaction with reactive molecules and corresponding N-reduction products evolution. However, in order to further investigate on the dynamics of the oxygen incorporation (re-oxidation of the catalysts), an accurate analysis of the experiments can be performed from a different point of view. In this sense, the catalytic performances can be discussed, as well, in terms of the oxidation degree achieved by the catalyst during the course of the experimental reaction steps. For this purpose, several calculations were made and compiled in Table 3 as well.

Since the nitrogen balance is closed, after finishing the consecutive reaction steps, by applying the following equation (8), the final amount of oxygen incorporated in the catalyst (O_{in}) can be estimated, according to the reaction mechanisms possibly taking place, see Reactions (4-7). It could be checked that whatever the sequence of steps performed for every catalyst, a similar oxidation degree is achieved by the catalyst.

$$(O_{in}) = 1 \cdot \sum N_2O + 2 \cdot \sum N_2 \qquad (8)$$

By accomplishing the same calculations with ceria-zirconia, pre-reduced at 450°C, similar final amounts of oxygen are incorporated as well (after both sequences of reaction), but in a lower extent than those achieved by Cu2/CZ (Table 3).

Figure 16 represents the progress of the catalysts' oxidation during the course of the catalytic steps as oxygen incorporated onto the catalyst in terms of reaction time. In this sense, faster oxidation kinetics due to NO reduction can be observed for copper/ceria-zirconia at 250°C than those at 50°C. By completing the NO-TPR step, the measurements of oxygen incorporated into the catalysts can be considered as convergent. Similar trends can be seen for ceria-zirconia. It is worth noting that very similar NO total amounts were reduced during the whole experiment (considering both isothermal stage and final heating ramp), since the key factor governing this process is the population of oxygen vacancies created. When oxygen vacancies are exhausted, the reaction is finished. Very interestingly, by tentatively assuming that all the hydrogen consumed during the pre-reduction step creates an active site (a reduced position on the catalyst), the estimations show that the efficiency of these oxygen vacancies as active sites in the generation of reduced N-products is very high (around 90%) for Cu2CZ. In the case of CZ, the

efficiency of the oxygen vacancies as main active sites is lower, but still satisfactory (around 60%). It is assumed that these active sites (oxygen vacancies) in the catalysts are being filled during the course of the reaction, when they interact with NO until saturation of the catalysts.

4. Conclusions

The main conclusions derived from this work, devoted to the study at a fundamental level of the NO reduction with ceria-based catalysts after conditioning and reduction in H_2, are the following:

• The results of *in situ* XRD characterization indicate that neither particle sintering nor phase segregation phenomena were detected after the thermal treatments (conditioning in inert atmosphere and reduction in H_2) prior to the NO reaction.

• The presence of copper in the catalyst formulation promotes the reducibility and formation of oxygen vacancies, which are clearly involved in the NO reduction process. The combined analysis of the evidences provided but *in situ* DRIFTS data (previous and during the NO reaction), the *in situ* Raman spectra, (after pre-reduction step), and the catalytic data during all the steps of the reaction lead to establish the primary role of the oxygen vacancies in this context.

• CZ and Cu2CZ catalysts are reactive in the NO reduction reaction under the simplified and controlled experimental conditions selected for this study. However, CZ requires a more drastic pre-reduction step (450ºC) to achieve high conversions of NO to N_2 and N_2O. Besides, the N_2/N_2O emission ratio, during this step, strongly depends on the NO reaction temperature.

• There is a complex network of reactions occurring at the catalysts' surfaces involving fast consumption of vacancies by NO reaction and ad-NOx species formation.

There are strong evidences pointing out that the route involving hydroxyls consumption takes place.

• The *in situ* DRIFTS technique has been revealed as an extremely interesting surface characterization technique to monitor the surface transformations during the different reaction steps that allow us to elucidate the main pathways of the NO reduction process onto ceria-based catalysts.

• The reduction of NO under the sequence of steps performed (isothermal reaction and NO-TPR) can be understood as the progress of the catalyst's oxidation with time, taking place at higher rates, with predominant N_2 emission at higher temperatures. Once the vacancies have been consumed, independently on the sequences of NO reaction, the emission of N-reduced products finishes. The efficiency of the created vacancies/active sites, during the pre-reduction step towards this process, is very high.

Acknowledgements

The authors gratefully acknowledge the financial support of Generalitat Valenciana (PROMETEO/2018/076 project) and the Spanish Ministry of Science, Innovation and Universitites (CTQ2015-64801-R project) and the UE-FEDER funding. Martínez-Munuera also acknowledges Spanish Ministry of Science, Innovation and Universities for the financial support through a FPU grant (FPU17/00603). Prof. García wants to thank the Research Services at the University of Alicante (SSTTI) for in situ XRD and Raman analysis.

5. References

[1] Y. Bisaiji, K. Yoshida, M. Inoue, K. Umemoto, T. Fukuma, SAE Int. J. Fuels Lubr. 5 (2011) 380–388.

[2] T.V. Johnson, A. Joshi, *In Catalysis Series Nº. 33, NOx Trap Catalysts and Technologies: Fundamentals and Industrial Applications,* Eds. L. Lietti, L. Castoldi., The Royal Society of Chemistry, 2018, pp 1-35.

[3] A. Reihani, B. Patterson, J. Hoard, G.B. Fisher, J.R. Theis, C.K. Lambert, J. Eng. Gas Turbines Power 139 (2017) 102805–102811.

[4] L. Yang, V. Franco, A. Campestrini, J. German, P. Mock, in: ICCT White Pap., Search PubMed, 2015.

[5] A. Reihani, G.B. Fisher, J.W. Hoard, J.R. Theis, J.D. Pakko, C.K. Lambert, Appl. Catal. B Environ. 223 (2018) 177–191.

[6] M. Inoue, Y. Bisaiji, K. Yoshida, N. Takagi, T. Fukuma, Top. Catal. 56 (2013) 3–6.

[7] K. Yoshida, H. Kobayashi, Y. Bisaiji, N. Oikawa, T. Fukuma, Top. Catal. 59 (2016) 845–853.

[8] Y. Bisaji, K. Yoshida, in: L. Lietti, L. Castoldi (Eds.), NOx Trap Catal. Technol. Fundam. Ind. Appl., Catalysis Series Nº 33, 2018, pp. 408–411.

[9] G. Liu, P.-X. Gao, Catal. Sci. Technol. 1 (2011) 552–568.

[10] A. Bueno-López, K. Krishna, M. Makkee, J.A. Moulijn, J. Catal. 230 (2005) 237–248.

[11] Y. Wang, J.P. de Boer, F. Kapteijn, M. Makkee, Top. Catal. 59 (2016) 854–860.

[12] A. Trovarelli, P. Fornasiero, Catalysis by Ceria and Related Materials, Second Edi, Imperial College Press, 2013.

[13] A. Trovarelli, Catalysis by Ceria and Related Materials, Imperial College Press, London, 2002.

[14] Y. Wang, M. Makkee, Appl. Catal. B Environ. 223 (2018) 125–133.

[15] Y. Wang, J.P. de Boer, F. Kapteijn, M. Makkee, ChemCatChem 8 (2016) 102–105.

[16] Y. Wang, M. Makkee, Appl. Catal. B Environ. 221 (2018) 196–205.

[17] J. Giménez-Mañogil, A. Bueno-López, A. García-García, Appl. Catal. B Environ. 152–153 (2014) 99–107.

[18] J. Giménez-Mañogil, A. García-García, Appl. Catal. A Gen. 542 (2017) 226–

239.

[19] J.A. Sullivan, P. Dulgheru, I. Atribak, A. Bueno-López, A. García-García, Appl. Catal. B Environ. 108–109 (2011) 134–139.

[20] M. Adamowska, S. Muller, P. Da Costa, A. Krzton, P. Burg, Appl. Catal. B Environ. 74 (2007) 278–289.

[21] R. Di Monte, J. Kašpar, J. Mater. Chem. 15 (2005) 633–648.

[22] A. Davó-Quiñonero, M. Navlani-García, D. Lozano-Castelló, A. Bueno-López, J.A. Anderson, ACS Catal. 6 (2016) 1723–1731.

[23] B. Azambre, L. Zenboury, A. Koch, J.V. Weber, J. Phys. Chem. C 113 (2009) 13287–13299.

[24] Z. Wu, M. Li, J. Howe, H.M. Meyer, S.H. Overbury, Langmuir 26 (2010) 16595–16606.

[25] T. Taniguchi, T. Watanabe, N. Sugiyama, A.K. Subramani, H. Wagata, N. Matsushita, M. Yoshimura, J. Phys. Chem. C 113 (2009) 19789–19793.

[26] M. Guo, J. Lu, Y. Wu, Y. Wang, M. Luo, Langmuir 27 (2011) 3872–3877.

[27] M. Daturi, N. Bion, J. Saussey, J.-C. Lavalley, C. Hedouin, T. Seguelong, G. Blanchard, Phys. Chem. Chem. Phys. 3 (2001) 252–255.

[28] C. Binet, M. Daturi, J.-C. Lavalley, Catal. Today 50 (1999) 207–225.

[29] G.N. Vayssilov, M. Mihaylov, P.S. Petkov, K.I. Hadjiivanov, K.M. Neyman, J. Phys. Chem. C 115 (2011) 23435–23454.

[30] A. Laachir, V. Perrichon, A. Badri, J. Lamotte, E. Catherine, J.C. Lavalley, J. El Fallah, L. Hilaire, F. Le Normand, E. Quéméré, G.N. Sauvion, O. Touret, J. Chem. Soc. Faraday Trans. 87 (1991) 1601–1609.

[31] E. Finocchio, M. Daturi, C. Binet, J.C. Lavalley, G. Blanchard, Catal. Today 52 (1999) 53–63.

[32] M. Piumetti, S. Bensaid, D. Fino, N. Russo, Appl. Catal. B Environ. 197 (2016) 35–46.

[33] M.Y. Mihaylov, E.Z. Ivanova, H. a. Aleksandrov, P. St. Petkov, G.N. Vayssilov, K.I. Hadjiivanov, Appl. Catal. B Environ. 176–177 (2015) 107–119.

[34] M. Daturi, E. Finocchio, C. Binet, J.C. Lavalley, F. Fally, V. Perrichon, J. Phys. Chem. B 103 (1999) 4884–4891.

[35] H. Knözinger, P. Ratnasamy, Catal. Rev. 17 (1978) 31–70.

[36] C. Binet, A. Badri, J.-C. Lavalley, J. Phys. Chem. 98 (1994) 6392–6398.

[37] G.S. Ofelt, J. Phys. Chem. 37 (1962) 511–520.

[38] B. Azambre, I. Atribak, A. Bueno-López, A. García-García, J. Phys. Chem. C 114 (2010) 13300–13312.

[39] K.I. Hadjiivanov, Catal. Rev. Sci. Eng. 42 (2000) 71–144.

[40] I. Atribak, B. Azambre, A. Bueno López, A. García-García, Appl. Catal. B Environ. 92 (2009) 126–137.

[41] V.I. Pârvulescu, P. Grange, B. Delmon, Catal. Today 46 (1998) 233–316.

[42] Y. Chi, S.S.C. Chuang, J. Catal. 190 (2000) 75–91.

[43] L. Liu, J. Cai, L. Qi, Q. Yu, K. Sun, B. Liu, F. Gao, L. Dong, Y. Chen, J. Mol. Catal. A Chem. 327 (2010) 1–11.

LIST OF TABLES

Table 1. Lattice parameters and average crystal sizes obtained from *in situ* XRD measurements.

	CZ		Cu2CZ	
Steps	**Lattice parameter* (nm)**	**Average crystal size* (nm)**	**Lattice parameter* (nm)**	**Average crystal size* (nm)**
1) 25ºC Ar	0.535	8.2	0.535	8.0
2) 300ºC (10 min) Ar	0.539	7.0	0.533	7.1
3) 400ºC (10 min) Ar	0.539	7.4	0.537	7.8
4) 500ºC (10 min) Ar	0.539	7.3	0.536	7.3
5) 500ºC (30 min) Ar	0.536	7.5	0.539	7.3
6) 350ºC Ar	0.537	7.2	0.539	7.5
7) 350ºC (30 min) H_2/Ar	0.540	7.0	0.539	7.7
8) 350ºC (60 min) H_2/Ar	0.539	7.3	0.539	7.6
9) 25ºC H_2/Ar	0.536	7.5	0.539	7.8

* Lattice parameters and average crystal sizes were estimated by using the main (111) peak reflection of ceria-zirconia.

Table 2. Reaction data obtained during isothermal NO reaction.

NO reaction (isothermal step)					
Catalyst *	**Temperature (ºC)**	**NO consumed ($\mu mol/g_{cat}$)**	**N_2O produced ($\mu mol/g_{cat}$)**	**N_2 produced ($\mu mol/g_{cat}$)**	**N_2O/N_2 ratio**
Cu2/CZ (350ºC)	50	784	328	55	6.5
Cu2/CZ (350ºC)	250	852	81	310	0.3
CZ (450ºC)	50	360	131	24	5.5
CZ (450ºC)	250	179	23	80	0.3
CZ (350ºC)	50	62	3	5	0.6
CZ (350ºC)	250	45	5	7	0.7

* Pre-reduction temperature of each sample shown in parenthesis.

Table 3. Quantifications of the products released during the experiments, hydrogen consumption during pre-reduction and oxygen incorporated onto the catalysts. Pre-reduction of CZ was conducted at 450ºC and Cu2CZ at 350ºC.

	NO-TPR step		Total quantification **		Pre-reduction		
Catalyst *	**N_2O produced ($\mu mol/g_{cat}$)**	**N_2 produced ($\mu mol/g_{cat}$)**	**$\sum N_2O$ produced ($\mu mol/g_{cat}$)**	**$\sum N_2$ produced ($\mu mol/g_{cat}$)**	**H_2 consumption ($\mu mol/g_{cat}$)**	**O incorporated onto the catalyst (µmol/gcat)**	**Efficiency *** (%)**
Cu2/CZ (50ºC)	107	114	435	169	859	773	90
Cu2/CZ (250ºC)	1	3	82	313		708	82
CZ (50ºC)	7	20	138	44	344	226	65
CZ (250ºC)	1	11	24	91		206	60

* Temperature of the isothermal NO reaction step of each sample shown in parenthesis.

** Sum of the N_2O or N_2 produced during the isothermal NO reaction step (see Table 2) and the subsequent NO-TPR.

*** Efficiency of the "active sites" in the generation of reduced N-products.

LIST OF FIGURES

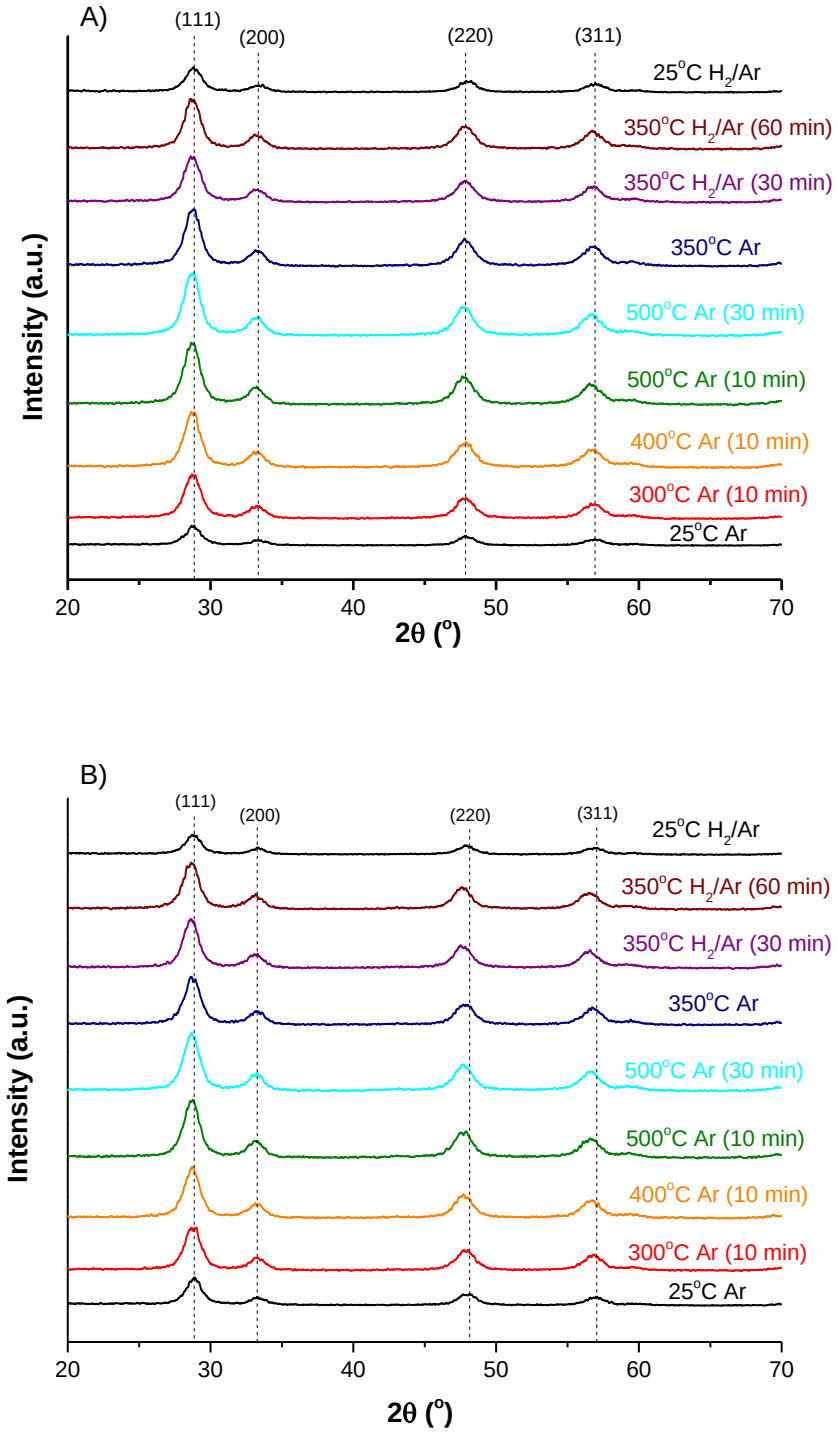

Figure 1. X-ray diffractograms of the pre-treatment and pre-reduction stages for the samples: A) CZ, and B) Cu2CZ.

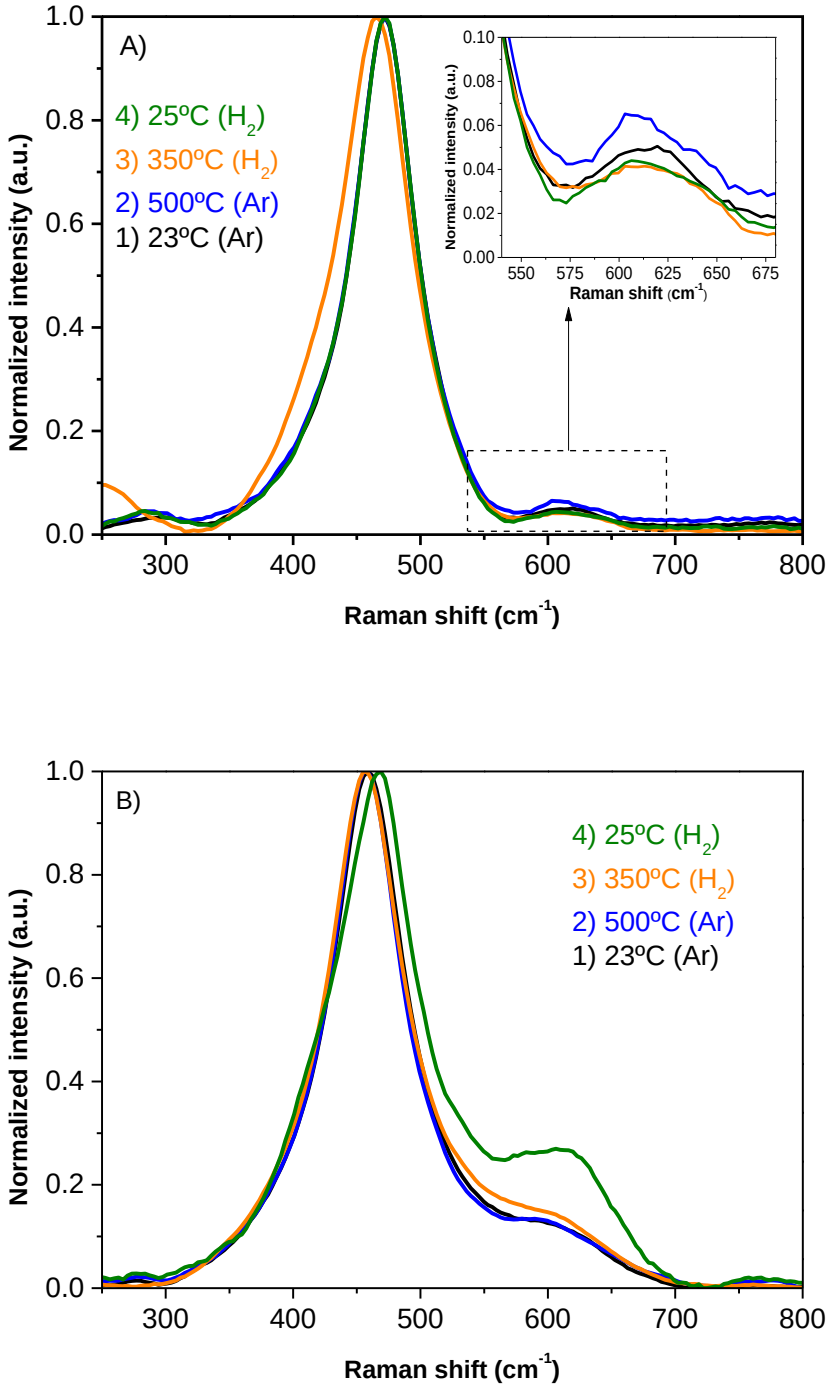

Figure 2. Normalized Raman spectra of the pre-treatment and pre-reduction stages for the samples: A) CZ, and B) Cu2CZ.

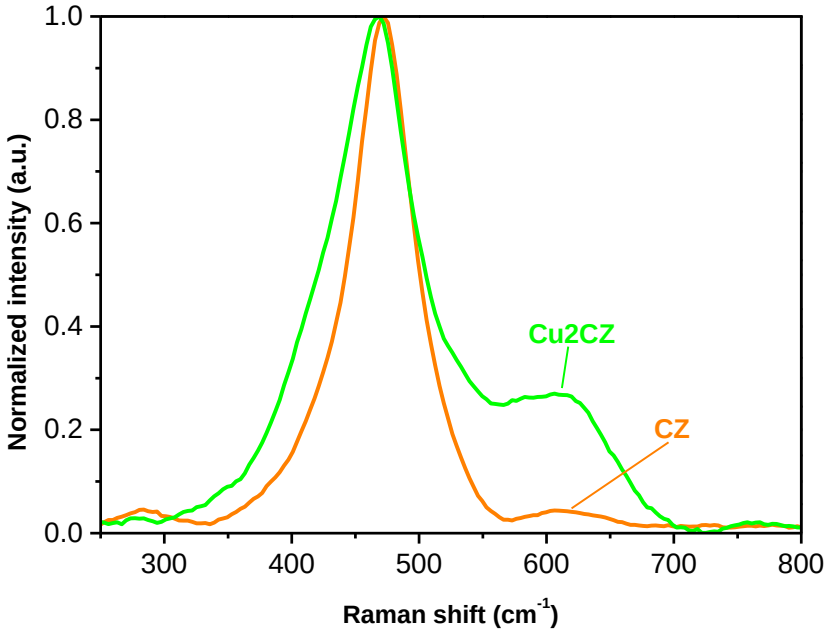

Figure 3. Normalized Raman spectra, registered at 25ºC, under H_2, after pre-reduction of the catalysts, for comparative purposes.

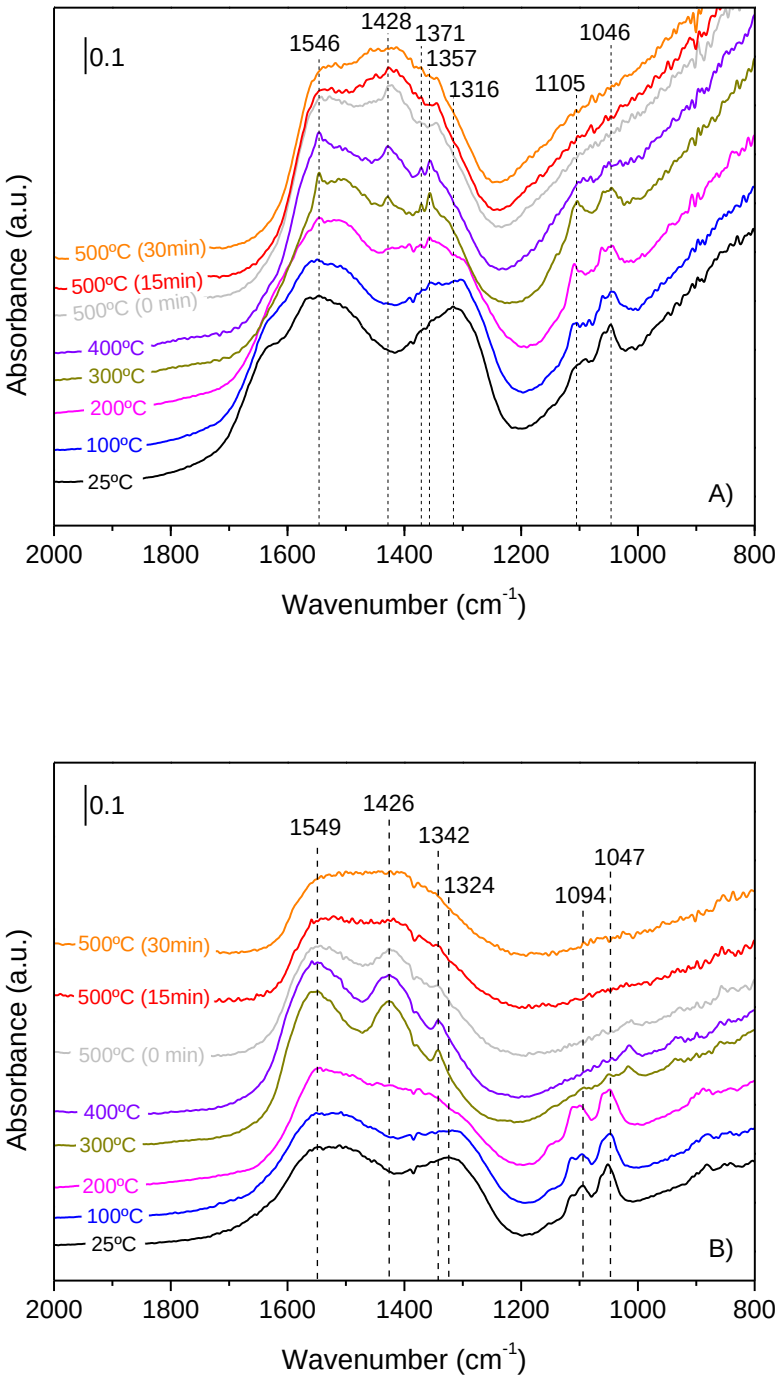

Figure 4. DRIFTS spectra during the pre-conditioning stage under N_2, in the region of 2000-800 cm^{-1} for the catalysts: A) CZ, and B) Cu2CZ.

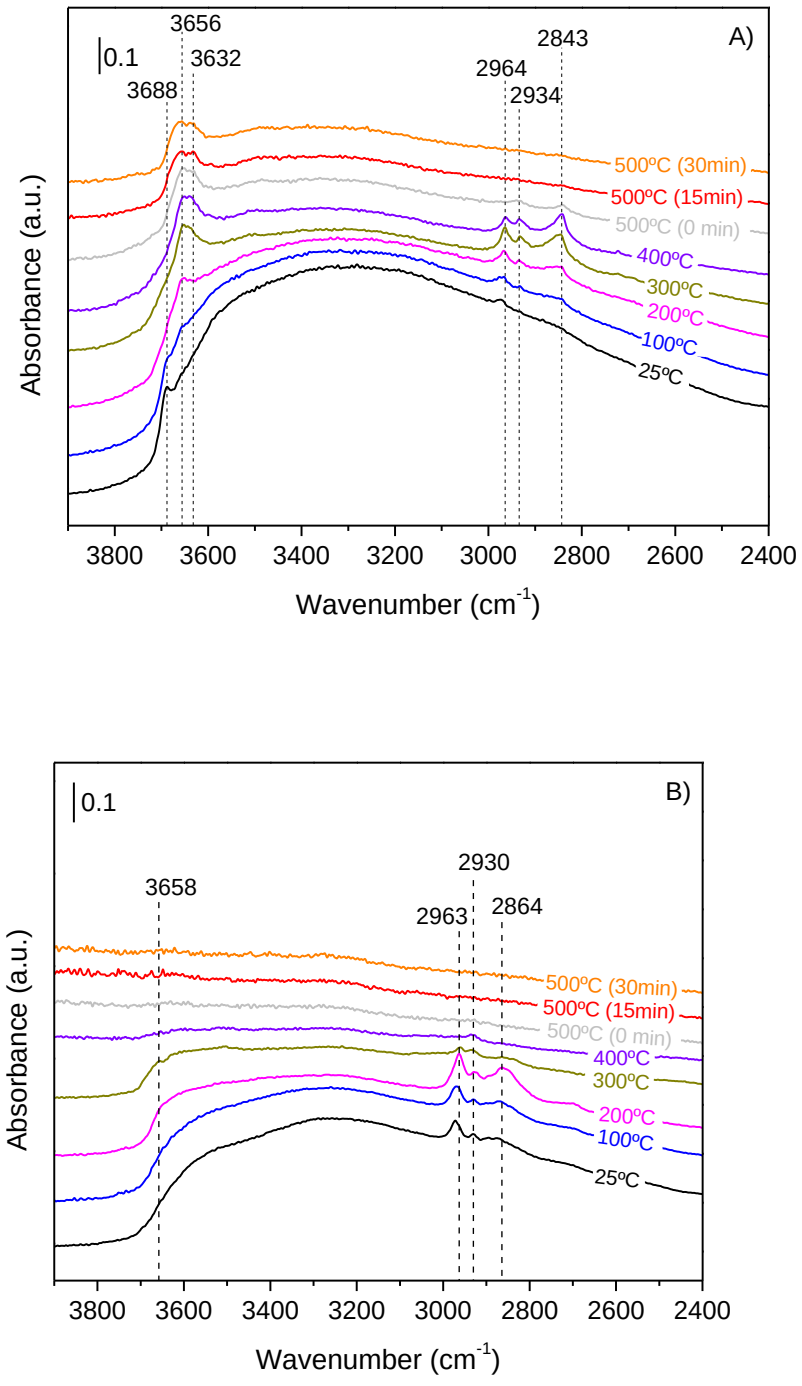

Figure 5. DRIFTS spectra during the pre-conditioning stage under N_2, in the region of 3900-2400 cm^{-1} for the catalysts: A) CZ, and B) Cu2CZ.

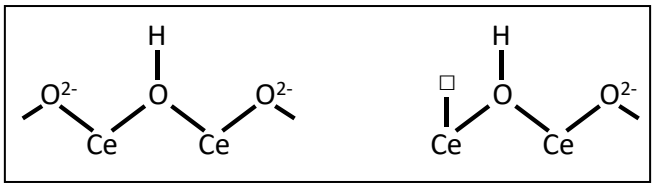

Figure 6. Scheme of type II-A hydroxyl group (left) and type II-B group (right) on the ceria surface, where □ symbol represents an oxygen vacancy.

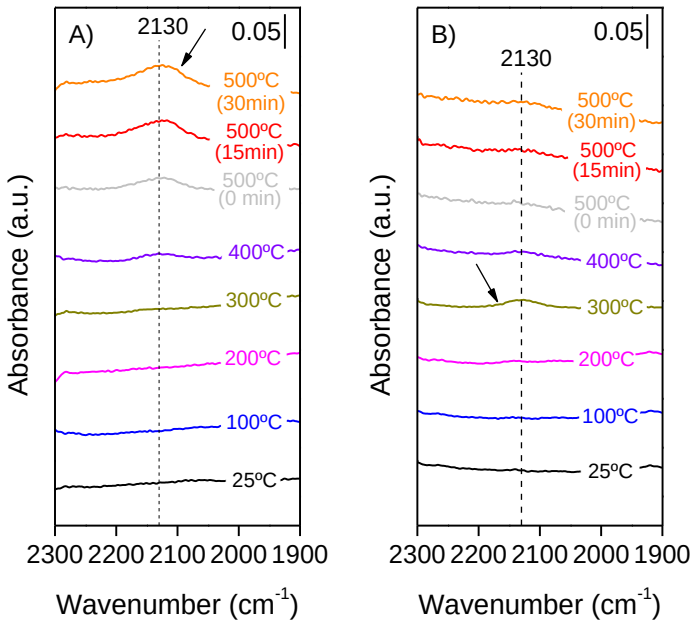

Figure 7. DRIFTS spectra during the pre-conditioning stage under N_2, in the region of 2300-1900 cm^{-1} for the catalysts: A) CZ, and B) Cu2CZ. The arrows included in the Figures point the oxygen vacancies band.

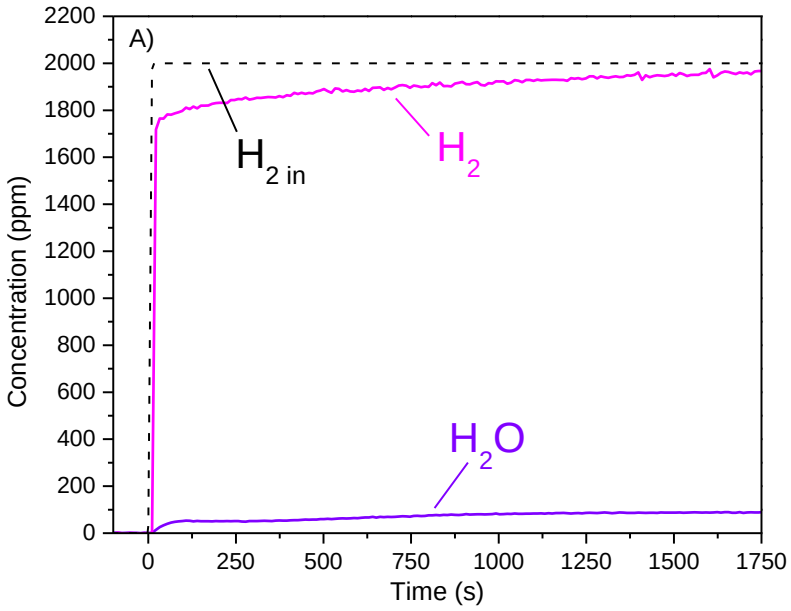
A)
$H_{2\ in}$
H_2
H_2O
Concentration (ppm)
Time (s)
0
200
400
600
800
1000
1200
1400
1600
1800
2000
2200
0
250
500
750
1000
1250
1500
1750

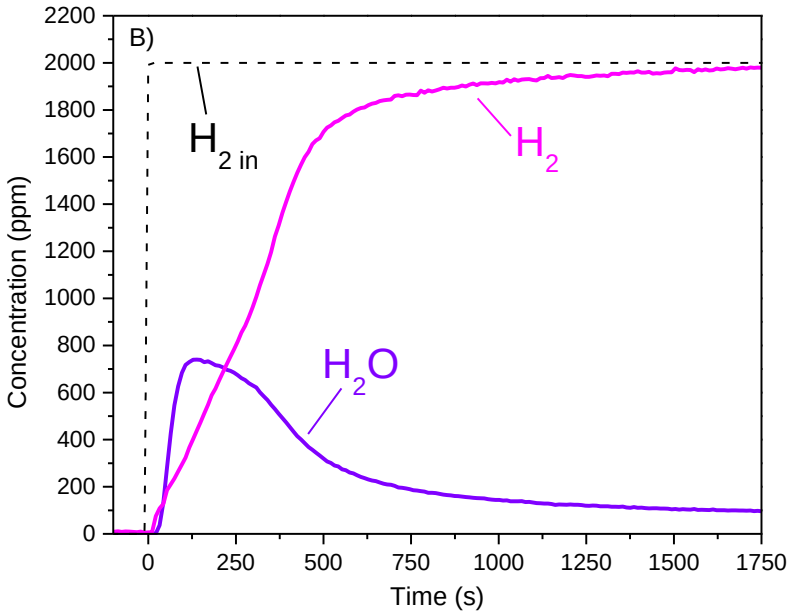
B)
$H_{2\ in}$
H_2
H_2O
Concentration (ppm)
Time (s)
0
200
400
600
800
1000
1200
1400
1600
1800
2000
2200
0
250
500
750
1000
1250
1500
1750

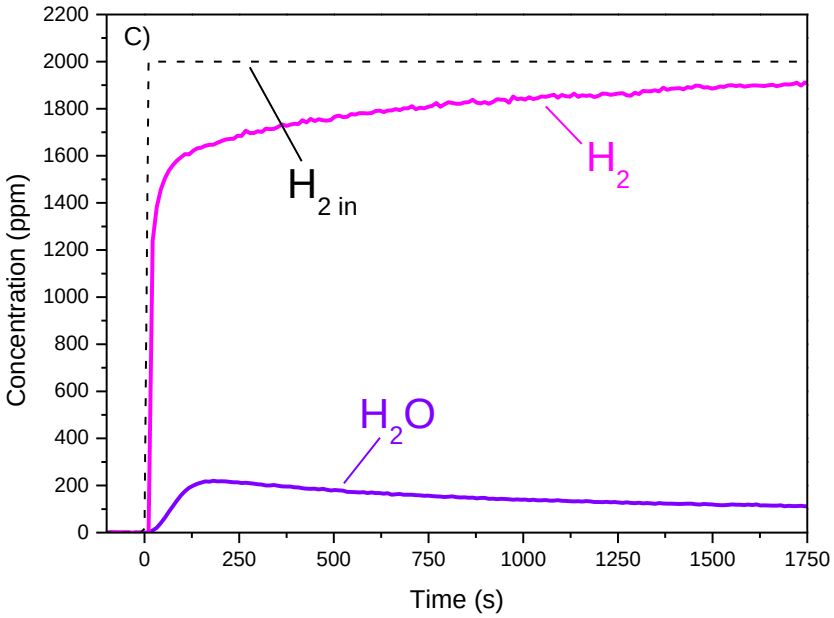

Figure 8. H_2 and H_2O concentration profiles during the pre-reduction step along the catalytic activity tests, for the catalysts at the corresponding temperature (in parenthesis): A) CZ (350ºC), B) Cu2CZ (350ºC) and C) CZ (450ºC).

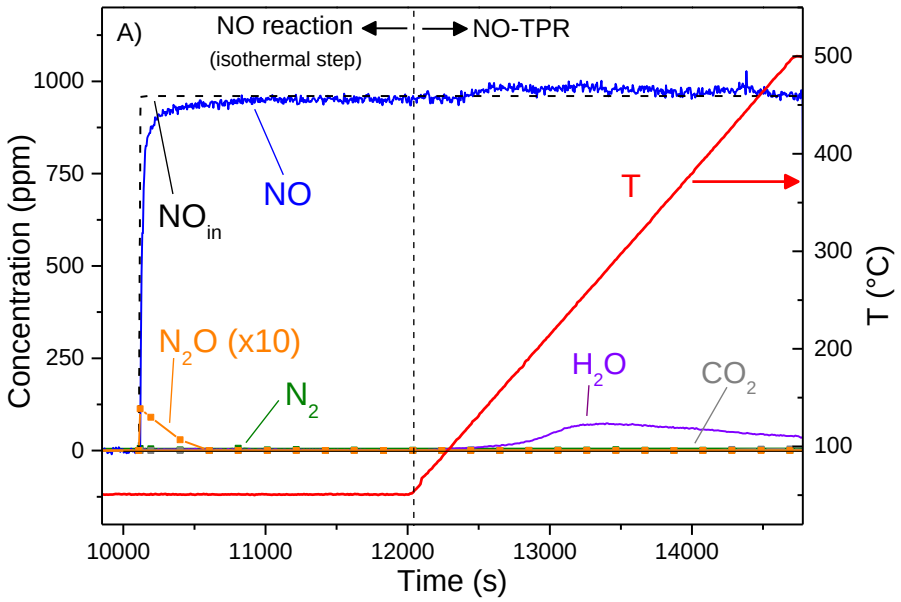
A)
NO reaction
(isothermal step)
NO-TPR
Concentration (ppm)
T (°C)
Time (s)
NO
NO_in
N2O (x10)
N2
H2O
CO2
T

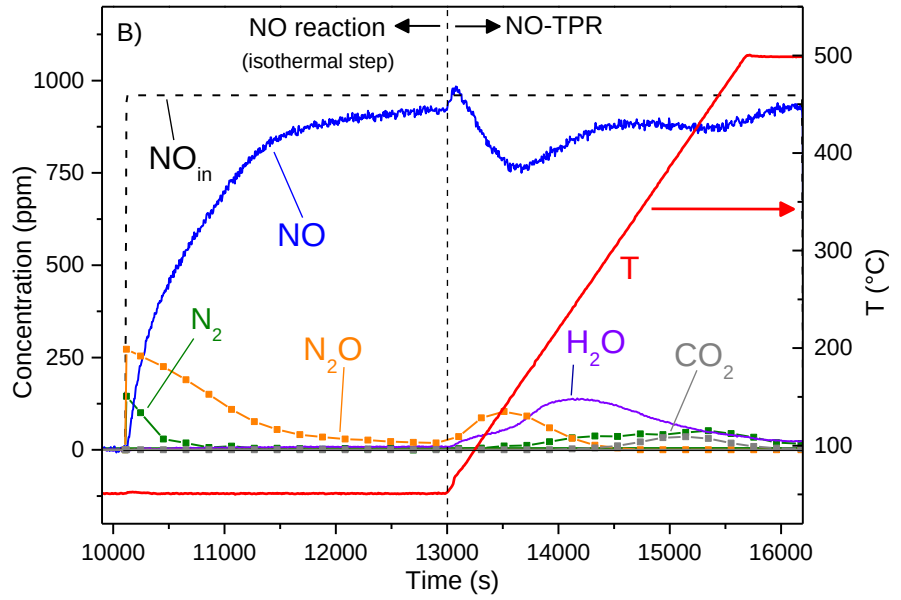
B)
NO reaction
(isothermal step)
NO-TPR
Concentration (ppm)
T (°C)
Time (s)
NO_in
NO
N2
N2O
H2O
CO2
T

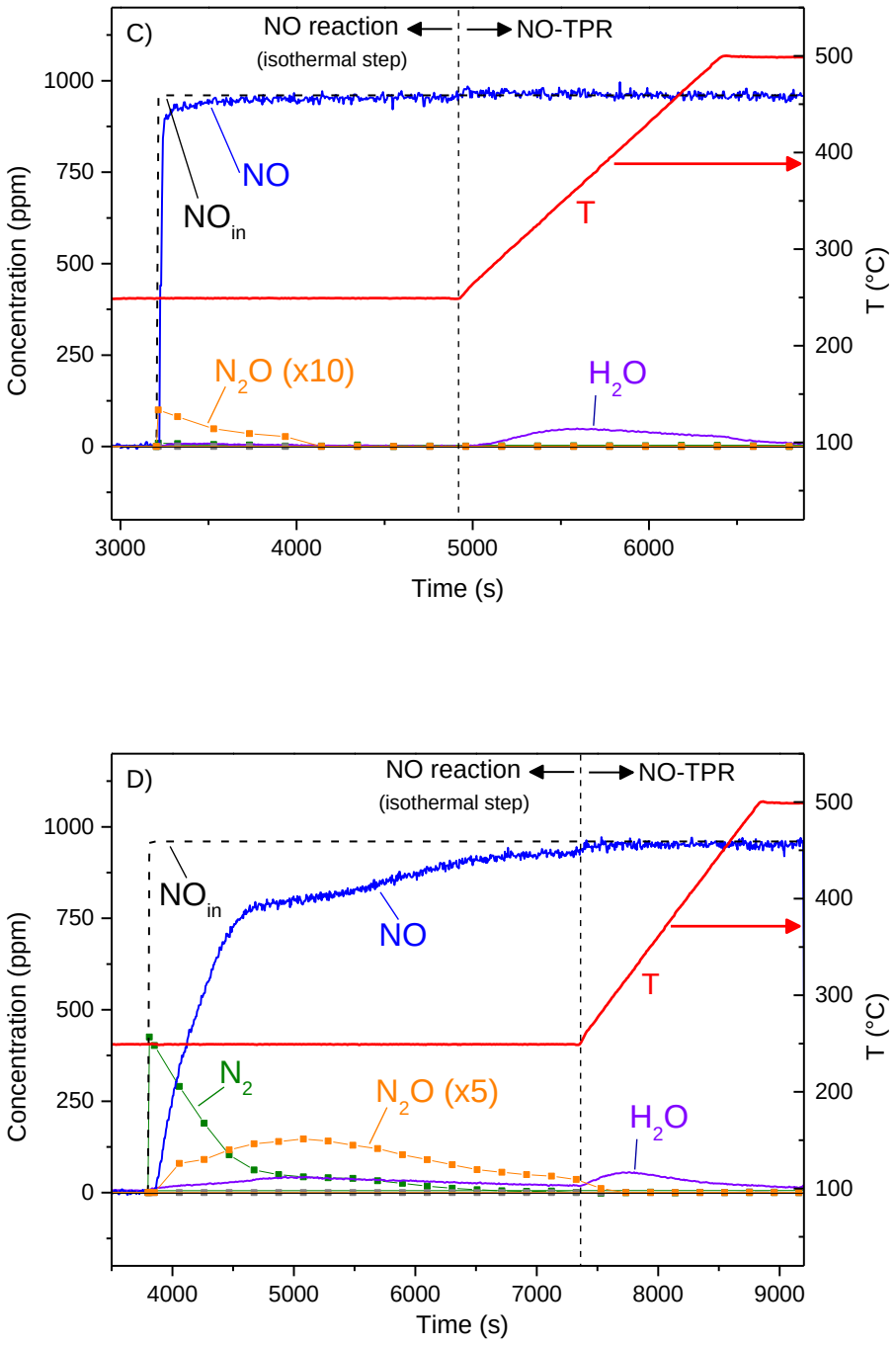

Figure 9. Concentration profiles of different species during the isothermal NO reaction and NO-TPR steps in the catalytic activity tests, after pre-reduction of the catalysts at 350ºC, at the corresponding temperature (in parenthesis): A) CZ (50ºC), B) Cu2CZ (50ºC) C) CZ (250ºC) and D) Cu2CZ (250ºC).

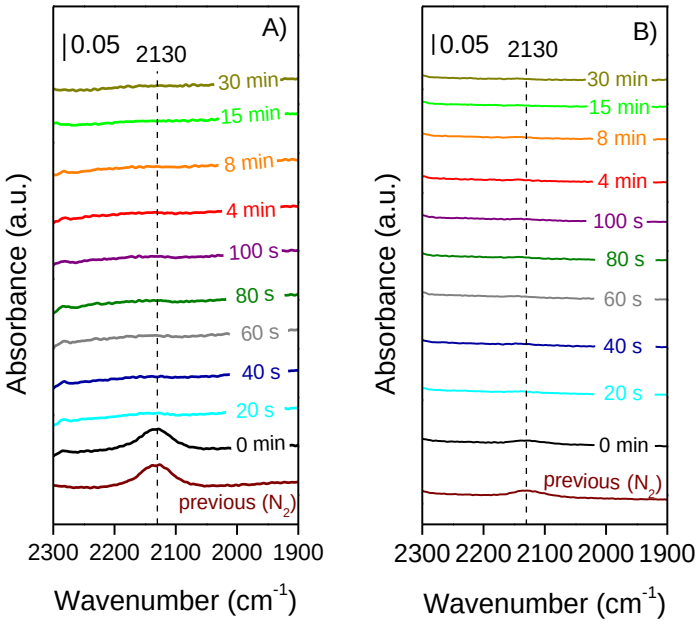

Figure 10. DRIFTS spectra during the isothermal NO reaction stage (at 50ºC), in the region of 2300-1900 cm^{-1} for the catalysts: A) CZ, and B) Cu2CZ.

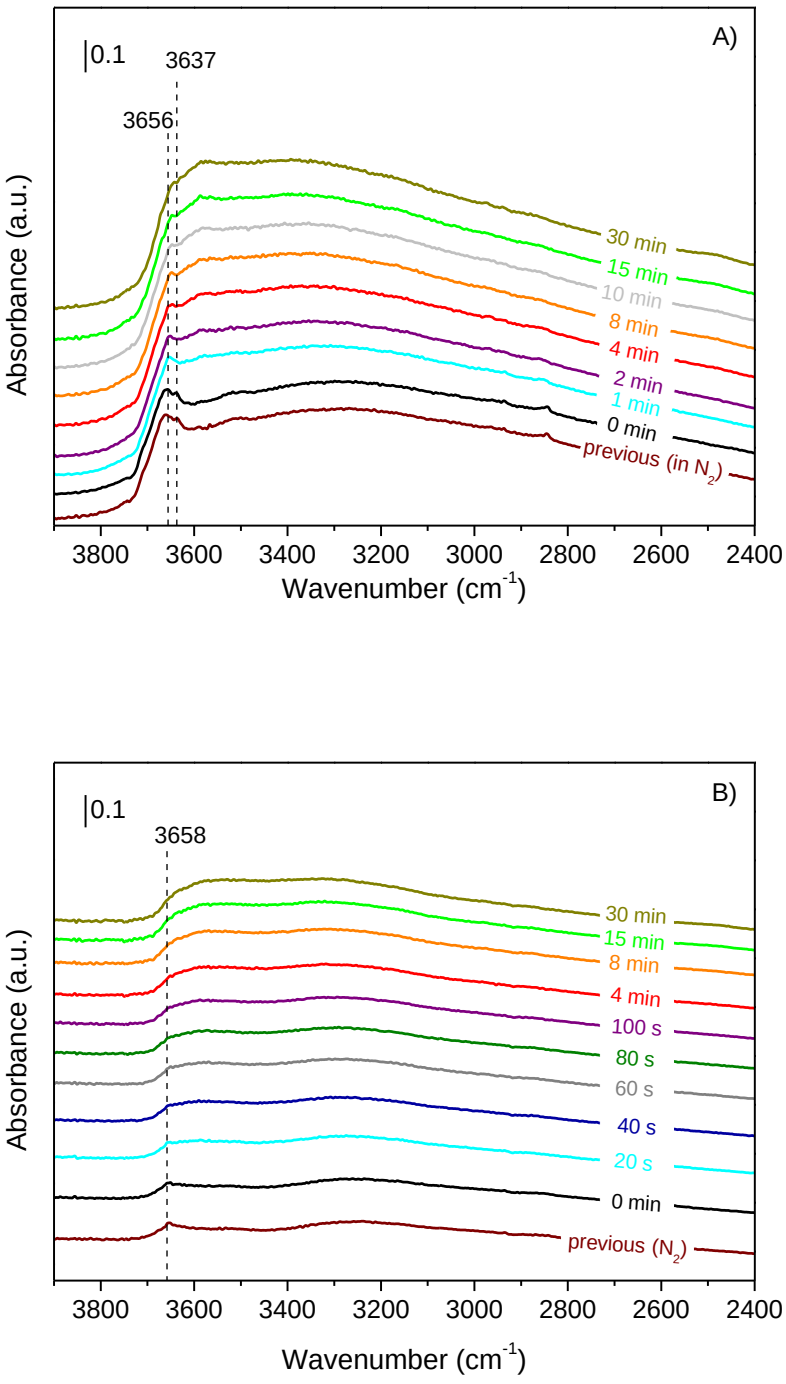

Figure 11. DRIFTS spectra during the isothermal NO reaction stage (at 50ºC), in the region of 3900-2400 cm^{-1} for the catalysts: A) CZ, and B) Cu2CZ.

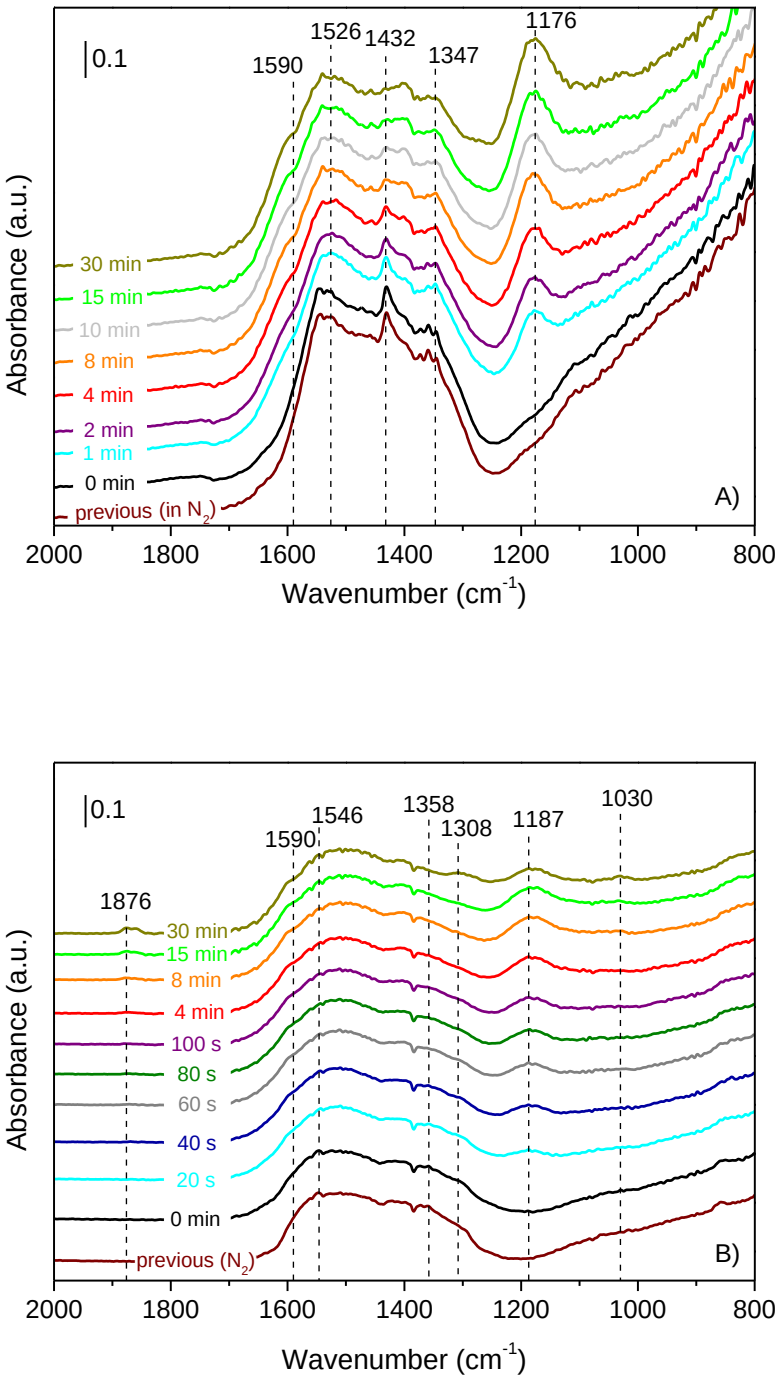

Figure 12. DRIFTS spectra during the isothermal NO reaction stage (at 50ºC), in the region of 2000-800 cm^{-1} for the catalysts: A) CZ, and B) Cu2CZ.

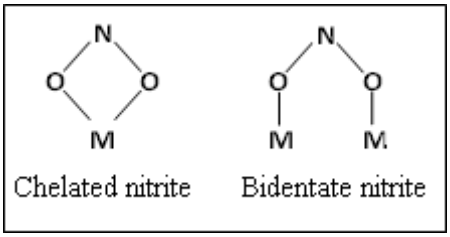

Figure 13. Scheme of chelated nitrite species (left) and bidentate nitrite species (right), detected by DRIFTS.

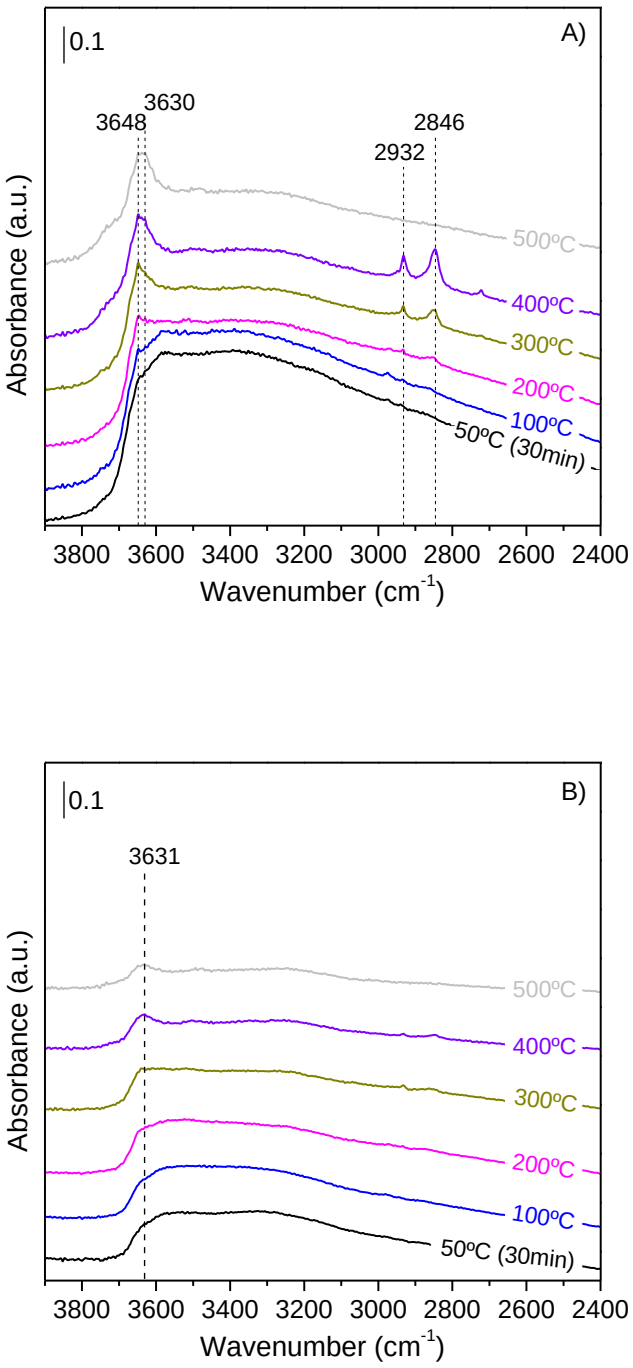

Figure 14. DRIFTS spectra at different temperatures during the final NO-TPR stage (after isothermal NO reaction at 50ºC), in the region of 3900-2400 cm^{-1}. A) CZ and B) Cu2CZ.

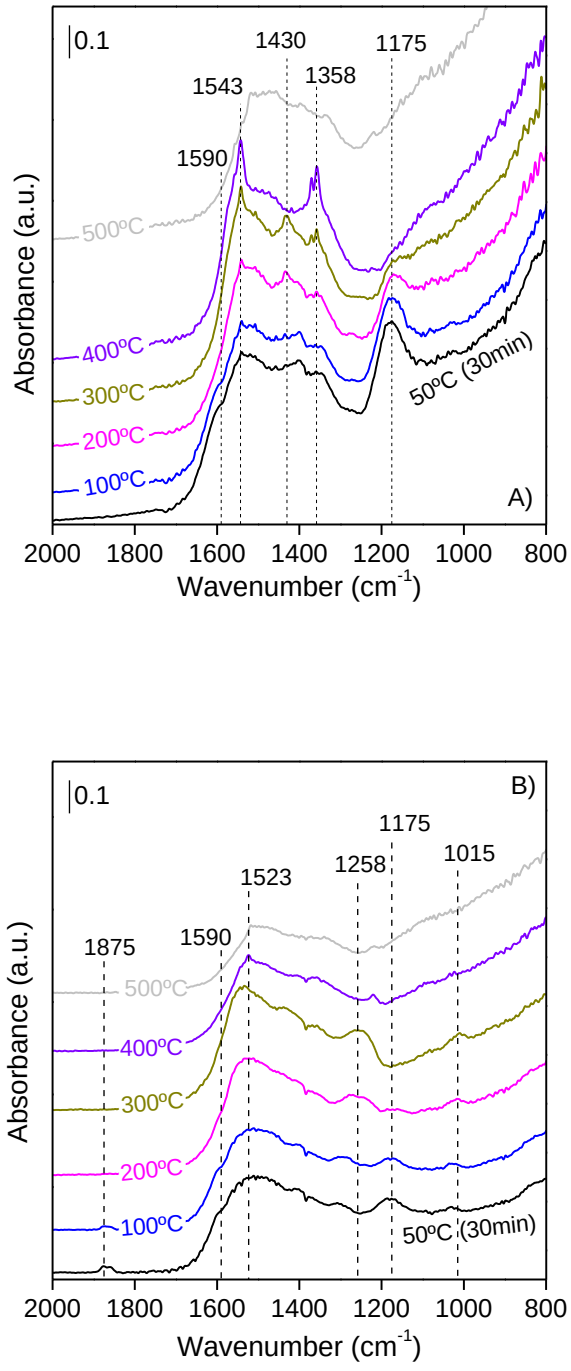

Figure 15. DRIFTS spectra at different temperatures during the final NO-TPR stage (after isothermal NO reaction at 50ºC), in the region of 2000-800 cm^{-1}. A) CZ and B) Cu2CZ.

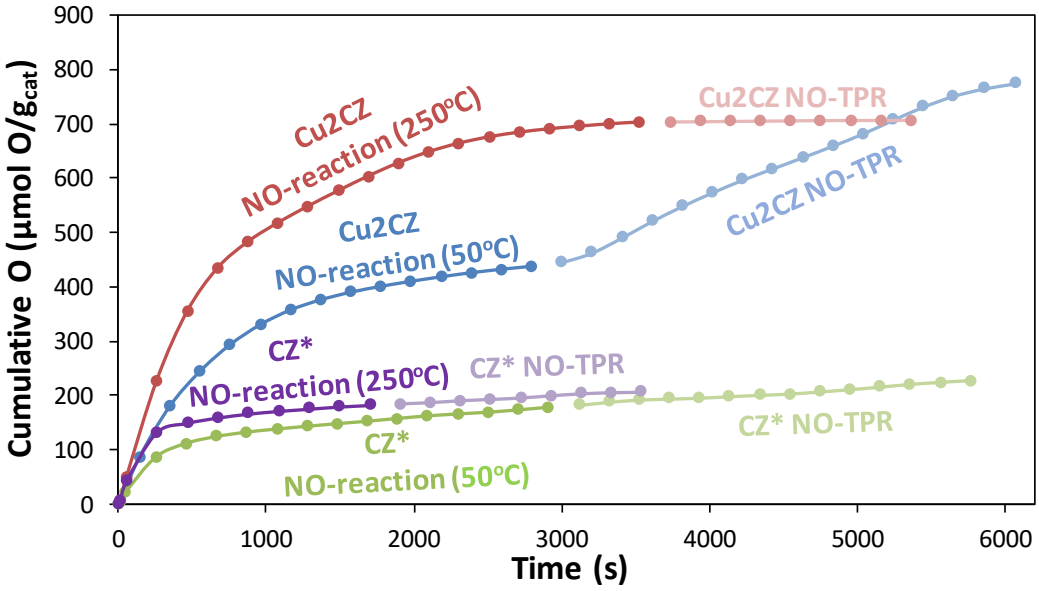

Figure 16. Cumulative oxygen curves of the catalysts (as a consequence of re-oxidation of the catalysts) during the different experimental stages –O_{in}-. (Cu2CZ was pre-reduced at 350ºC and CZ* at 450ºC).